Quantitative X-Ray Diffraction From Superlattices

Eric E. Fullerton, Ivan K. Schuller, and
Y. Bruynseraede

NATIONAL LABORATORY

ARGONNE

UNIVERSITY OF CHICAGO

MRS BULLETIN REPRINT

Quantitative X-Ray Diffraction From Superlattices

Eric E. Fullerton, Ivan K. Schuller, and
Y. Bruynseraede

Introduction

The physical properties of superlattices have been the subject of considerable interest because a wide range of phenomena associated with very thin films, interfaces, and coupling effects can be studied.[1] Recent areas of activity in metallic superlattices include antiferromagnetic coupling of ferromagnetic layers across nonmagnetic spacer layers,[2] giant magnetoresistance,[3] magnetic surface anisotropy,[4] low-dimensional superconductivity,[5-6] and anomalous mechanical properties.[7] All of these phenomena are strongly affected by the chemical and physical properties of the individual layers and by the superlattice structure. Therefore, a detailed understanding of the properties of superlattices requires a nondestructive, *quantitative* determination of the superlattice structure.

Because superlattices are not in thermodynamic equilibrium, their structure is sensitive to preparation methods and growth conditions. A dramatic example of superlattice structural dependence on growth conditions is shown in Figure 1, for sputtered Nb/Si superlattices.[8] Increasing the Ar pressure during sputtering decreases the kinetic energy of the deposited atoms,[9] thereby changing their surface mobility, and thus altering growth dynamics. Figure 1 shows the low-angle x-ray diffraction and cross-sectional transmission electron microscopy (TEM) images of $[Nb(35\ \text{Å})/Si(25\ \text{Å})]_{40}$ superlattices sputtered in, respectively, 3 and 15 mTorr of Ar. The TEM image of the 3 mTorr superlattice clearly shows the smooth and continuous layering across the entire cross section of the image ($\approx 5\ \mu m$). This is characteristic of sputtered metal/semiconductor superlattices used for x-ray optics.[10] The TEM observations are confirmed by the low-angle x-ray-diffraction spectrum where peaks are observed up to high order with no obvious broadening of the diffraction lines. The structure for the superlattice grown at 15 mTorr is quite different. The initial layers appear smooth and as growth progresses, the layer roughness increases, forming parabolic growth fronts characteristic of low surface mobility and self-shadowing.[11] Only limited low-angle x-ray diffraction peaks are observed and the line widths are broadened as a result of cumulative layer-thickness fluctuations.[12]

The effects of structural disorder on the physics of the superlattice will depend on the particular property of interest. In maximizing the reflectivity of an x-ray mirror, the effects of increasing the Ar pressure, and consequently increasing the roughness will clearly degrade performance. In the case of giant magnetoresistance effects in Fe/Cr superlattices, which is dominated by interface scattering, increased roughness at the interface enhances the magnetic scattering.[13] The elastic properties of Nb/Si superlattices are found to be independent of the roughness.[14] Other structural properties which are also important include interdiffusion, crystal structure and orientation, lattice strains, interfacial crystalline coherence, and defects in the layers.

X-Ray Diffraction

A complete quantitative characterization of the superlattice requires a determination of the morphology, chemistry, and crystal structure of the layers. In this aspect, x-ray diffraction proves to be a powerful technique. It is easy to use, fast, nondestructive, and provides information both at the atomic scale and from correlations over thousands of angstroms. The most commonly used scattering geometry are reflectivity measurements in which the scattering vector is normal to the lay-
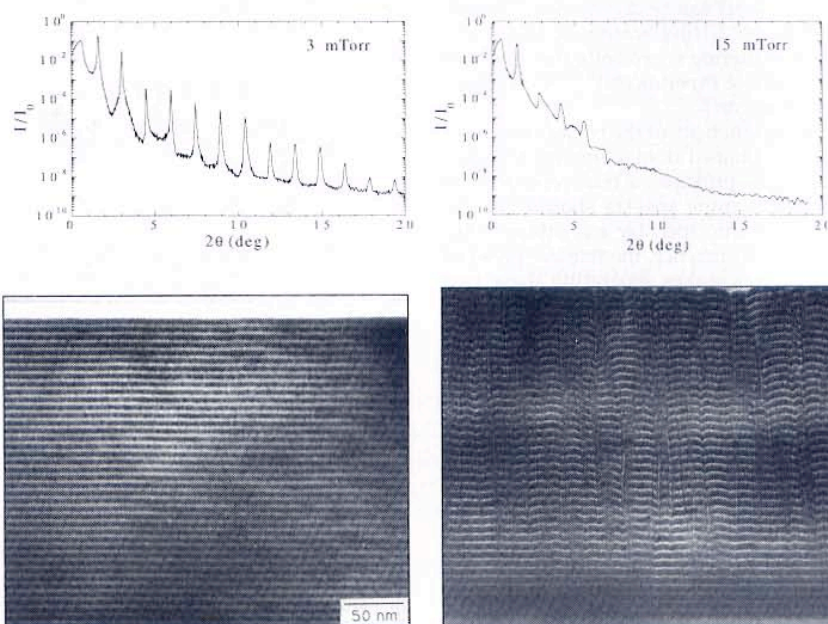

Figure 1. Low-angle x-ray-diffraction spectra and transmission electron microscopy image of $[Nb(35\ \text{Å})/Si(25\ \text{Å})]_{40}$ superlattices sputtered in an Ar pressure of 3 mTorr (left panels) and 15 mTorr (right panels).

ers. Reflectivity measurements are conventionally separated between the "low" angle ($<20°$) (shown in Figure 1) and "high" angle ($>20°$) regions of the spectra.

In the low-angle region, the length scales studied are greater than the lattice spacings of the constituent layers, so the scattering can be considered as arising solely from the chemical modulation of the structure. The low-angle spectra are usually modeled using an optical theory in which the scattering from the superlattice is calculated recursively, adding sequentially the reflectivity of each interface.[15,16] When considering the scattering from a rough surface or interface, the scattered intensity usually can be separated into specular and diffuse components.[17,18] By performing a rocking curve or transverse scan in which the scattering vector is out of the specular condition, the diffuse scattering can be measured. To determine the true specular scattering, the diffuse scattering has to be subtracted from the measured reflectivity.[17] Fitting model calculations to the specular component gives the interdiffusion and average roughness of the interfaces. At this stage we should point out that it has been common to fit scattering intensity using a Debye-Waller formalism, although, strictly speaking, this is incorrect.[19] By fitting the transverse scans of the diffuse scattering, the lateral coherence, frequency, and correlation of the interface roughness from layer to layer can be determined.[19] Modeling of the diffuse scattering from low-angle scattering is presently the subject of considerable experimental[17,18,20,21] and theoretical research.[22]

Information about the crystal structures can be obtained from scattering at higher angles. In principle, a transverse scan of the high-angle spectra should also be separable into specular and diffuse components. In practice, the mosaic spread of crystallites makes separating these two components impossible. In this case, a reflectivity measurement is effectively proportional to a measurement of integrated intensity, since transverse scan-line widths associated with mosaic spreads are independent of the particular reflection scanned. To compare the measured intensities with calculated intensities requires computing the total scattering intensity (specular and diffuse). The total or integrated intensity is given by an average $<FF^*>$ where F is the scattering factor of the superlattice and $<...>$ indicates an ensemble average over all possible superlattice structures. The specular intensity alone is given by $<F><F^*>$.[23] An experimental demonstration of the difference between the specular and integrated

intensities was recently shown for scattering from ErAs films epitaxially grown on GaAs.[23,24] For thin layers, a specular and a diffuse component are separable in the transverse scan about the (002) reflection, which allows the determination of the specular reflectivity. For thicker layers, only a single line in the transverse scan characteristic of mosaic spread was observed. For the latter case, the measured reflectivity could only be fit by an expression for the integrated intensity.

A general kinematic formula for the scattered intensity of a superlattice can be derived for both specular and integrated intensities.[25] The scattering factor for a superlattice with M bilayers is given by:

$$F = \sum_{j=1}^{M} \exp(iqx_j)\,[F_{Aj} + \exp(iqt_{Aj})F_{Bj}] \quad (1)$$

where x_j is the distance from the substrate and the jth bilayer, F_{Aj} (F_{Bj}) is the scattering factor for constituent A (B) in the jth bilayer and t_{Aj} (t_{Bj}) are the corresponding layer thicknesses including interface spacing. If the layer fluctuations are statistically independent, the scattering intensity for the specular and integrated intensities can be written:

$$I_{spec} = |\langle F \rangle|^2$$

$$= \left| \frac{1 - (T_A T_B)^M}{1 - T_A T_B}(\bar{F}_A + T_A \bar{F}_B) \right|^2 \quad (2)$$

$$I_{int} = \langle FF^* \rangle$$

$$= M[I_A + 2\,\mathrm{Re}[\Phi_A \bar{F}_B] + I_B] +$$

$$2\,\mathrm{Re}\left[\left\{ \frac{\Phi_B \bar{F}_A}{T_A T_B} + \frac{\Phi_A \bar{F}_A}{T_A} + \frac{\Phi_B \bar{F}_B}{T_B} \right. \right.$$

$$\left. + \Phi_A \bar{F}_B \right\}$$

$$\cdot \left\{ \frac{M - (M+1)T_A T_B + (T_A T_B)^{M+1}}{(1 - T_A T_B)^2} \right.$$

$$\left. \left. - M \right\} \right] \quad (3)$$

where Re designates the real part of the term in the bracket, and the following averaged quantities of the individual layers are given by:

$$I_A = \langle F_A F_A^* \rangle, \quad I_B = \langle F_B F_B^* \rangle$$

$$\bar{F}_A = \langle F_A \rangle, \quad \bar{F}_B = \langle F_B \rangle$$

$$\Phi_A = \langle \exp(iqt_A)F_A^* \rangle, \quad \Phi_B = \langle \exp(iqt_B)F_B^* \rangle$$

$$T_A = \langle \exp(iqt_A) \rangle, \quad T_B = \langle \exp(iqt_B) \rangle \quad (4)$$

The angled brackets now represent ensemble averages over individual layers.

The specific definition of the scattering factor and ensemble averages depends on the superlattice system studied and the types of disorder (see Reference 25 for specific examples).

The peak positions of the high-angle diffraction spectra are dependent only on the average lattice spacing of the constituent layers and the modulation wavelength Λ. Structural information of the constituent layers requires modeling the superlattice structure (including lattice strains, interdiffusion, and disorder) and comparing the calculated diffraction intensities of the model with the measured intensities. By adjusting the structural parameters of the model to best fit the measured intensities, structural parameters of the layers can be quantitatively refined.[25-28] This type of structural characterization of complex structures from bulk powder materials are commonly performed using the Rietveld refinement procedure.[29] There is an important difference between refinement of superlattice structures and the standard Rietveld refinement. The calculation of Equation 3 determines the line shapes as well as the relative intensities, so the entire diffraction spectrum is fit with the structural model. In Rietveld refinement, the structure of a single unit is modeled to determine relative intensities, and measured line shapes are fit to structural independent profiles.

The structural model used in the refinement depends on the particular system, but in general they include the following features:

■ Lattice strains within each constituent layer. The layer is described by a lattice spacing in the center of the layer, and deviations from this lattice spacing near each interface.

■ An average number of atomic planes in each layer and discrete (integer number of atomic planes) fluctuations about the average layer thickness.

■ Continuous atomic level disorder at each interface or within the layer.

■ Chemical interdiffusion at each interface.

Because the growth of material A onto B and B onto A may not be equivalent, the parameters of the A-B and B-A interface can be refined separately.

Applications of Structural Refinement

We will now discuss the application of the superlattice refinement procedure to a number of superlattice systems where different parameters affected the x-ray diffraction spectra. These include sputtered Nb/Cu and high T_c superlattices and Ag/Mn superlattices grown by molecular

Table I: Refined Roughness Values Compared to the Artificial Roughness for a Series of Nb/Cu Superlattices.

$S_{Artificial}(\mathring{A})$*	$S_{Refined}(\mathring{A})$*	
	Nb(110)/Cu(111)	Nb(220)/Cu(222)
$S_{Nb} = 0.0$, $S_{Cu} = 0.0$	$S_{Nb} = 1.0$, $S_{Cu} = 3.7$	$S_{Nb} = 1.0$, $S_{Cu} > 3.0$
$S_{Nb} = 0.0$, $S_{Cu} = 1.9$	$S_{Nb} = 1.0$, $S_{Cu} = 4.7$	$S_{Nb} = 1.3$, $S_{Cu} > 3.0$
$S_{Nb} = 0.0$, $S_{Cu} = 2.8$	$S_{Nb} = 1.0$, $S_{Cu} = 5.1$	$S_{Nb} = 1.0$, $S_{Cu} > 3.0$
$S_{Nb} = 2.8$, $S_{Cu} = 0.0$	$S_{Nb} = 1.0$, $S_{Cu} = 3.2$	$S_{Nb} = 2.6$, $S_{Cu} > 3.0$
$S_{Nb} = 3.8$, $S_{Cu} = 0.0$	$S_{Nb} = 2.7$, $S_{Cu} = 3.2$	$S_{Nb} > 3.0$, $S_{Cu} > 3.0$

*$S_{Artificial}$ and $S_{Refined}$ are the standard deviation of discrete layer thickness fluctuations introduced during growth and determined by the refinement procedure respectively.
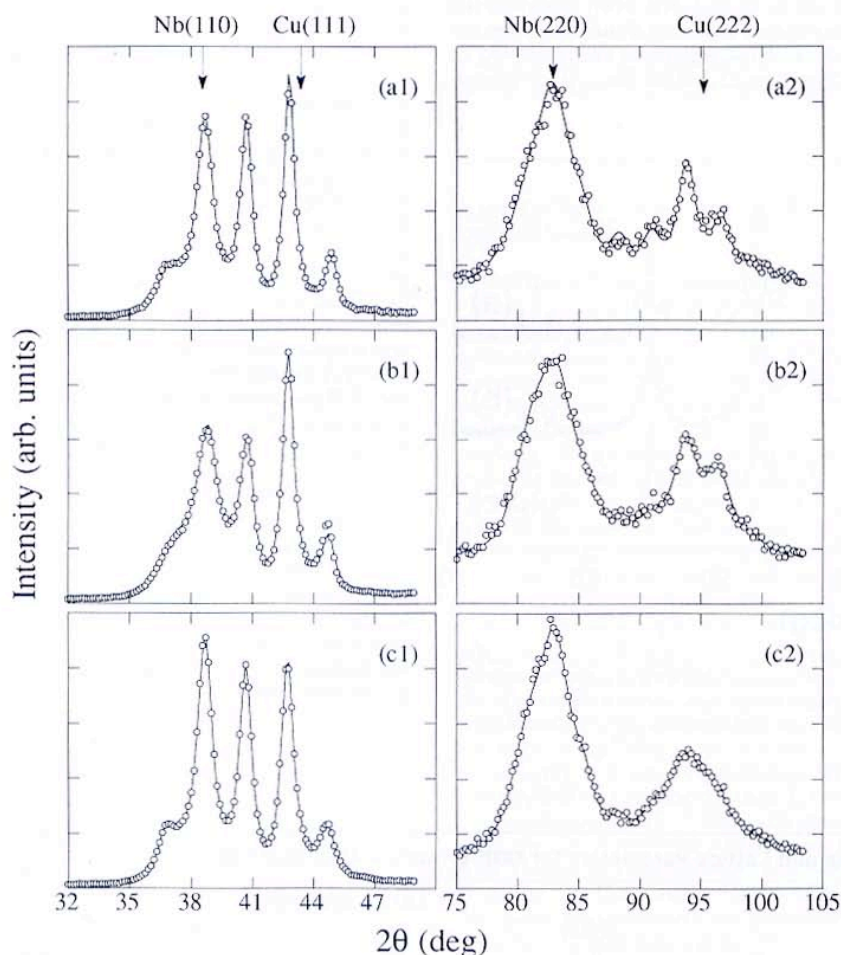

Figure 2. Experimental (open circles) and refined (full line) high-angle x-ray-diffraction spectra for three [Nb(26 Å)/Cu(20 Å)]$_{40}$ superlattices: (a) without artificial roughness, (b) with 2.8 Å artificial roughness on the Cu layers, and (c) 2.8 Å artificial roughness on the Nb layers. The spectra on the left are taken around the first-order Bragg reflections and the spectra on the right around the second order. All spectra are plotted on a linear scale and are normalized to the highest intensity.

beam epitaxy. Particular emphasis is placed on quantitative comparison of refined parameters from the method described above with independent determination of the same structural parameters.

Layer Thickness Fluctuations in Nb/Cu Superlattices

Crystalline-crystalline superlattices are expected to exhibit lateral discrete layer thickness fluctuations resulting from deviation from layer-by-layer growth and the deposition of a non-integer number of atomic planes in one layer.[30] In order to determine the sensitivity of x-ray diffraction to layer thickness fluctuations, a series of Nb/Cu superlattices were grown with layer thickness fluctuations introduced during sample growth. To introduce disorder into the layer thicknesses, the deposition time of the Nb and Cu were varied randomly from layer to layer so that the layer thicknesses approximated a Gaussian distribution about the average layer thickness. It is well-known that Nb/Cu superlattices can be grown as superlattices with the Nb(110) and Cu(111) planes oriented perpendicular to the substrate plane.[31] X-ray diffraction scans were performed about the first order (bcc(110)/fcc(111)) and the second order (bcc(220)/fcc(222)) regions of the spectra. Figure 2 shows the x-ray diffraction spectra from a series of [Nb(26 Å)/Cu(20 Å)]$_{40}$ superlattices with no artificially introduced layer thickness fluctuations (Figure 2a) and 2.8 Å of additional thickness fluctuations added to Cu (Figure 2b) and Nb (Figure 2c). The results of the discrete layer-thickness fluctuations as determined by x-ray refinement are given in Table I.

In the sample with no additional disorder (Figure 2a), the superlattice peaks about the Nb position are considerably broader than the peaks about the Cu position, which indicates that there is more discrete disorder in the Cu layers (contrary to what one may expect naively).[12] No superlattice peaks are observed about the Nb(220) peaks. The disorder values determined from the refinement about the first-order profile are a continuous disorder of 0.3 Å per interface and a standard deviation of discrete layer-thickness fluctuations in the Nb (Cu) layers of 1.0 Å (3.7 Å). When additional artificial roughness is added to the Cu layers (Figure 2b), the superlattice peaks around the Nb(110) reflection clearly broaden; however, the peaks about the Nb(220) do not change much. The Cu layers are already so rough that the superlattice peaks about the Nb(220) are not resolved and the additional, artificial roughness cannot be determined. Only a lower bound on the discrete roughness
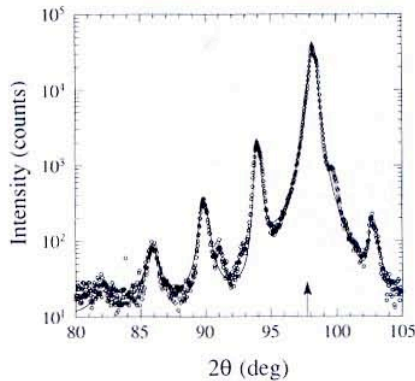
Figure 3. Experimental (open circles) and refined (full line) high-angle x-ray-diffraction spectrum for a [Ag(30 Å)/Mn(4 Å)]₆₀ superlattice. The arrow indicates the position of the additional Ag(004) buffer layer peak. The refined parameters are given in Table II.

Figure 4. X-ray diffraction spectra for a 2,000 Å c-axis oriented YBCO(4 u.c.)/GdBCO(4 u.c.) superlattice. (a) Perfect superlattice calculation, (b) experimental data, and (c) refined spectrum. The spectra were offset by three decades and the MgO substrate peak was deleted for clarity.

can be determined, as shown in Table I. With additional roughness added to the Nb layer (Figure 2c), the Nb and Cu layer roughness become comparable. This may lead to an uncertainty in the continuous and discrete disorder parameters from the refinement because both additions of roughness broaden the peaks, plus the limited number of higher-order satellite peaks limits the ability to resolve the disorder. As a consequence, the discrete disorder parameters are slightly lower than expected from the first-order profile results, with the consequent increase in the continuous roughness parameters.

The x-ray diffraction profiles shown in Figure 2 demonstrate that discrete disorder on the monolayer scale can be resolved for each constituent and that this needs to be included when modeling the superlattice structure. Similar experiments on Mo/Ni superlattices are presented in References 25 and 26. The relative intensi-

ties of the peaks are strongly dependent on the amount of layer-thickness fluctuations, even though the lattice parameters and average layer thicknesses remain constant. This shows that relative intensity calculations to determine the lattice parameters without roughness included in the model may give incorrect results.

Interfacial Strains in Ag/Mn Superlattices

An area of particular interest in the growth of thin films and superlattices is the growth of metastable phases and the manipulation of the atomic structure by epitaxial strain.[32] Considerable work has been done on the epitaxial growth of Mn in an attempt to stabilize a ferromagnetic phase. A series of MBE-grown epitaxial Ag/Mn superlattices and Mn films by Jonker et al.[33] were studied by reflection high-energy electron diffraction (RHEED),[33] extended x-ray-absorption fine-structure (EXAFS),[34] and x-ray photoelectron diffraction (XPD).[33] RHEED studies during growth determined that the Mn grows lattice matched in-plane to the Ag(001) surface. From the angle of the XPD forward-scattering peak, the lattice constant c/a ratio for the Mn films was determined, indicating it to be in a tetragonal phase. For Mn films five monolayers (ML) or greater, the out-of-plane spacing was estimated as 1.66 Å, which increased to 1.91 Å for thinner films. The comparison of these results to independent x-ray diffraction refinement on Ag/Mn superlattices using this method is described below.

Figure 3 shows the x-ray diffraction spectrum of a [Ag(30 Å)/Mn(4 Å)]₆₀ superlattice about the Ag(004) reflection, where the Mn thickness corresponds to approximately 2 ML. The open circles are the measured intensity and the line is a result of the refinement procedure. The refinement quantitatively reproduces the measured spectra over four orders of magnitude. The best results for the struc-
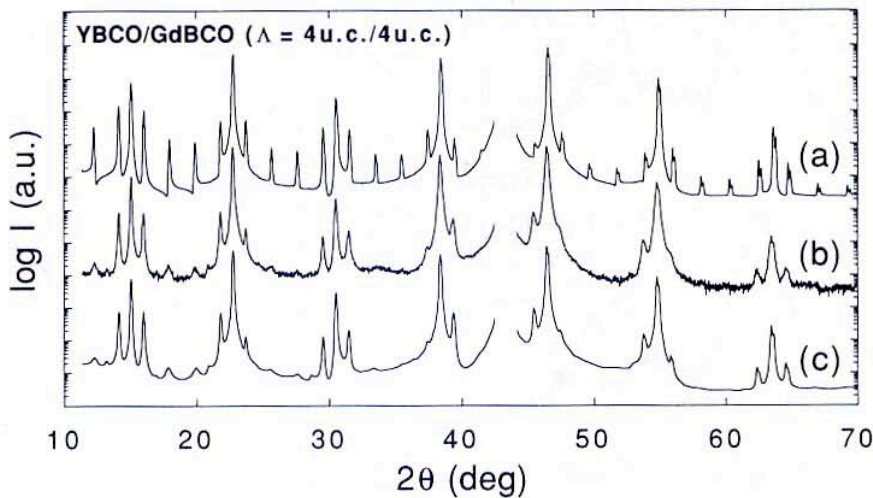
Table II: Refined Roughness and Lattice Parameters for MBE-grown Ag/Mn Superlattices.

| Thickness (monolayers) | | Roughness (Å) | | | Lattice Spacings (Å) | | | |
| | | | | | X-Ray | | EXAFS* | XPD* |
N_{Ag}	N_{Mn}	S_{Ag}	S_{Mn}	c	d_{Ag}	d_{Mn}	d_{Mn}	d_{Mn}
15	5	2	1	0.23	2.046±0.003	1.68±0.04	1.64±0.08	1.66
16	3	1	1	0.08	2.051±0.003	1.90±0.04	2.03±0.15	1.91
13	2	2	0.5	0.04	2.052±0.003	1.92±0.04	—	1.91

*XPD results are obtained from Reference 33 on Mn films, and EXAFS results on the same superlattices are obtained from Reference 34, where the Mn lattice spacings are estimated from the c/a ratio, assuming the in-plane lattice spacing is equal to the Ag lattice spacing.
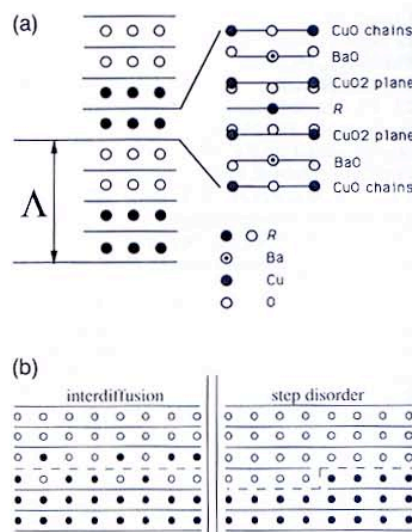
(a)

(b)

Figure 5. Top panel is the model for the perfect superlattice. White and black circles indicate the position of the alternating trivalent ions. Lines indicate the limits of the unit cells, whose structure is described as layers of CuO, BaO, CuO₂, and R with the proper interatomic spacing. For the unit cell schematic drawing the lines indicate the atomic plane position. Oxygen positions are properly placed with respect to the Cu and Ba atomic positions planes. Lower panel illustrates the two types of structural disorder included in the model. Interdiffusion assumes the R sites are randomly switched on either side of the interface, and the first unit cell away from the interface is treated as an Y123-Gd123 alloy. Step disorder assumes discrete fluctuations in the layer thicknesses of one unit cell.

Table III: Refinement Parameters for Selected High T_c Films and Superlattices.

Sample	$\bar{N}$ (u.c.)[a]	Cu1-Ba (Å)[b]	Ba-Cu2 (Å)[b]	Cu2-R (Å)[b]	c-axis (Å)
YBCO bulk	—	2.147	1.994	1.697	11.676
GdBCO bulk	—	2.143	1.987	1.717	11.694
YBCO film	—	2.15(1)[d]	2.01(1)	1.70(1)	11.722(3)
GdBCO film	—	2.14(1)	2.01(1)	1.72(1)	11.746(3)
Y(4 u.c.)/Gd(4 u.c.)[c]	4.4	2.15(1)	2.03(2)	1.67(2)	11.70(1)
	3.7	2.15(1)	2.00(2)	1.73(2)	11.76(1)
Y(1 u.c.)/Gd(1 u.c.)[c]	1.1	2.16(1)	2.04(2)	1.64(2)	11.68(1)
	0.9	2.15(1)	1.99(2)	1.75(2)	11.78(1)

[a]$\bar{N}$ is the average number of unit cells for a constituent layer.

[b]Cu1-Ba, Ba-Cu2, and Cu2-R are the interplanar spacings separating the metal ions in the c-axis direction as shown in Figure 5. Cu1 and Cu2 represent the Cu sites in the chains and planes respectively.

[c]For the superlattices, the top number is for the YBCO layer and the bottom number is the GdBCO layer.

[d]Numbers in parentheses indicate uncertainties in the last digit, estimated from fluctuation in refinement results on different initial parameters and details of the refinement model. Discrete disorder and interdiffusion parameters are discussed in the text.

tural disorder and lattice spacings obtained from fitting about the Ag(002) and Ag(004) reflections are given in Table II. Included in Table II are the EXAFS and XPD results. Excellent agreement is found in the determination of the out-of-plane spacing for the Mn layer. All three techniques imply a large decrease in the Mn lattice spacing as the layer increases from three to five ML. These results are also in agreement with XPD results by Egelhoff et al.[35] for Mn growth on Ag. Simultaneously with the decrease in the Mn lattice spacing, a large increase in the continuous roughness parameter is found from the refinement, indicating increasing atomic level structural disorder. This result is also consistent with the EXAFS studies, which determined increased disorder with increased Mn layer thick-

nesses. For layers thicker than 14 ML, the films lose long-range order.

Disorder in High T_c Superlattices

There is a considerable body of work on superlattices in which one or both of the layers are superconducting.[5-6,36] Using the superlattice geometry, it is possible to study the effects of reduced dimensionality, proximity effects, and interlayer coupling. These studies have been extended to include superlattices of high T_c materials, in particular $YBa_2Cu_3O_{7-\delta}$/$PrBa_2Cu_3O_{7-\delta}$ (YBCO/PrBCO) where the superconducting transition temperature is dependent both on the YBCO and PrBCO layer thicknesses.[37,38] The layer thicknesses studied in high T_c superlattices are typically 1–8 unit cells and are significantly affected by the presence of the interfaces. The structural characterization techniques most often used are high-resolution electron microscopy[39] and x-ray diffraction.

The x-ray refinement procedure has been applied to a number of high T_c thin films and superlattices.[40] The x-ray spectrum for c-axis-oriented YBCO(4 u.c.)/GdBCO(4 u.c.) grown on MgO is shown in Figure 4b. The spectra consist of the (00l) peaks resulting from the periodicity of the high T_c unit cell, and satellite peaks about each of these peaks resulting from the modulation of the rare earth sites. Since the films and superlattices studied are c-axis oriented, the diffraction intensity can be modeled as a sum of a–b planes. A perfect high T_c superlattice is schematically shown in Figure 5a. The

structure is modeled as a stack of unit cells with the well-known layered structure of the 123 materials,[41,42] alternating the two different rare earth sites. The calculated spectrum for a perfect superlattice with each layer maintaining bulk lattice spacings is shown in Figure 4a. There are a number of significant discrepancies between the calculated (Figure 4a) and measured (Figure 4b) diffraction spectra. In particular, the relative intensities and line widths of the satellite peaks do not agree with the measured spectrum.

Accounting for these discrepancies requires inclusion of structural disorder and modification of the interplanar spacings to account for interfacial strains. Shown schematically in Figure 5b are two kinds of the disorder interdiffusion and discrete disorder, which have qualitatively different effects on the diffraction spectra. Discrete disorder results in local fluctuations in the periodicity and broadens the superlattice peaks, as was shown for Nb/Cu superlattice in Figure 2. Interdiffusion does not affect the periodicity but reduces the contrast between layers, resulting in decreased satellite-peak intensities without broadening.

The result for the x-ray refinement procedure—including interplanar distances between metal ions in the unit cell, interdiffusion, step disorder, and a small continuous fluctuation of the layer thickness—is shown in Figure 4c. The relative intensities and line width are quantitatively reproduced. The rare-earth site interdiffusion in the first interfacial unit cell

is 15% Gd(Y) in the Y(Gd) sites without interdiffusion past one unit cell. This value increases to 25–30% for a single layer consistent with interdiffusion from both interfaces. Steps of one unit cell about the average layer thickness are sufficient to broaden the satellite peaks. Similar results are obtained for YBCO/PrBCO superlattices. Shown in Table III are the refined parameters for the superlattice in Figure 4, a YBCO(1 u.c.)/GdBCO(1 u.c.) superlattice and thin films of each constituent. Given that the in-plane lattice area for GdBCO is larger than that for YBCO, the in-plane strains on the YBCO (GdBCO) layers should be expansive (compressive), giving rise to an out-of-plane compression (expansion). This in fact is observed in the refinement results compared with the thin-film values for the YBCO and GdBCO.

Conclusion

X-ray structural refinement provides a powerful nondestructive quantitative technique for determining the atomic structure and disorder of superlattices. Structural parameters including the lattice strains, interdiffusion, step disorder, and atomic level disorder can be determined. If combined with transmission or grazing incidence diffraction to determine in-plane lattice constants[43,44] and low-angle scattering—which is more sensitive to the morphology of the interface over long lateral-length scales—a complete structural determination of the superlattice structure is possible. Computer programs, instruction manuals, and relevant references can be obtained by writing directly to two of the authors (IKS, YB) of this paper.

References

1. For instance, see various articles in *Physics, Fabrication and Applications of Multilayered Structures*, edited by P. Dhez and C. Weisbuch (Plenum Press, New York, 1988); *Metallic Superlattices, Artificially Structured Materials*, edited by T. Shinjo and T. Takada (Elsevier, Amsterdam, 1987).
2. S.S.P. Parkin, *Phys. Rev. Lett.* **67** (1991) p. 3598.
3. M.N. Baibich, J.M. Broto, A. Fert, F. Nguyen Van Dau, F. Petroff, P. Etienne, G. Creuzet, A. Friederich, and J. Chazelas, *Phys. Rev. Lett.* **61** (1988) p. 2472.
4. B.N. Engel, C.D. England, R.A. Van Leeubuen, M.H. Wiedmann, and C.F. Falco, *Phys. Rev. Lett.* **67** (1991) p. 1910.
5. I.K. Schuller, J. Guimpel, and Y. Bruynseraede, *MRS Bulletin* **XV** (2) (1990) p. 29.
6. D. Neerinck, K. Temst, M. Baert, E. Osquiguil, C. Van Haesendonck, Y. Bruynseraede, A. Gilabert, and I.K. Schuller, *Phys. Rev. Lett.* **67** (1991) p. 2577.
7. I.K. Schuller, A. Fartash, E.E. Fullerton, and M. Grimsditch, in *Thin Films: Stresses and Mechanical Properties III*, edited by W.D. Nix, J.C. Bravman, E. Arzt, and L.B. Freund (Mater. Res. Soc. Symp. Proc. **239**, Pittsburgh, PA, 1992) p. 499.
8. E.E. Fullerton, J. Pearson, C.H. Sowers, S.D. Bader, X-Z. Wu, and S.K. Sinha, to be published.
9. K. Meyer, I.K. Schuller, and C.M. Falco, *J. Appl. Phys.* **52** (1981) p. 5803.
10. E. Spiller, in *Physics, Fabrication and Applications of Multilayered Structures*, edited by P. Dhez and C. Weisbuch (Plenum Press, New York, 1988) p. 271.
11. C. Tang, S. Alexander, and R. Bruinsma, *Phys. Rev. Lett.* **64** (1990) p. 772.
12. J-P. Locquet, D. Neerinck, L. Stockman, Y. Bruynseraede, and I.K. Schuller, *Phys. Rev. B* **39** (1989) p. 13338.
13. E.E. Fullerton, D.M. Kelly, J. Guimpel, I.K. Schuller, and Y. Bruynseraede, *Phys. Rev. Lett.* **68** (1992) p. 859.
14. E.E. Fullerton, M. Grimsditch, and I.K. Schuller, unpublished.
15. J.H. Underwood and T.W. Barbee, *Appl. Opt.* **20** (1981) p. 3027.
16. B. Vidal and P. Vincent, *Appl. Opt.* **23** (1984) p. 1794.
17. S.K. Sinha, *Physica B* **173** (1991) p. 25.
18. D.E. Savage, J. Kleiner, N. Schimke, Y.H. Phang, T. Jankowski, J. Jacobs, R. Kariotis, and M.G. Lagally, *J. Appl. Phys.* **69** (1991) p. 1411.
19. W. Sevenhans, M. Gijs, Y. Bruynseraede, H. Homma, and I.K. Schuller, *Phys. Rev. B* **34** (1986) p. 5955.
20. J.B. Kortright, *J. Appl. Phys.* **70** (1991) p. 3620.
21. M.K. Sanyal, S.K. Sinha, A. Gibaud, S.K. Satija, C.F. Majkrzak, and H. Homma, in *Interface Dynamics and Growth*, edited by K.S.

Liang, M.P. Anderson, R.F. Bruinsma, and G. Scoles (Mater. Res. Soc. Symp. Proc. **237**, Pittsburgh, PA, 1992) p. 393.
22. D.G. Stearns, *J. Appl. Phys.* **71** (1992) p. 4286.
23. P.F. Miceli in *Semiconductor Interfaces, Microstructures, and Devices: Properties and Applications*, edited by Z.C. Feng (Adam Hilger IOP Publishing, Bristol, 1992).
24. P.F. Miceli, C.J. Palmstrøm, and K.W. Moyers, to be published.
25. E.E. Fullerton, I.K. Schuller, H. Vanderstraeten, and Y. Bruynseraede, *Phys. Rev. B* **45** (1992) p. 9292.
26. I.K. Schuller, E.E. Fullerton, H. Vanderstraeten, and Y. Bruynseraede, *Structure/Property Relationships for Metal/Metal Interfaces*, edited by A.D. Romig, D.E. Fowler, and P.D. Bristowe (Mater. Res. Soc. Symp. Proc. **229**, Pittsburgh, PA, 1991) p. 41.
27. F.J. Lamelas, H.D. He, and R. Clarke, *Phys. Rev. B* **43** (1991) p. 12296.
28. G. Gladyszewski and P. Mikołajczak, *Appl. Phys. A* **48** (1989) p. 521.
29. H.M. Rietveld, *J. Appl. Cryst.* **2** (1969) p. 65.
30. D.B. McWhan, in *Physics, Fabrication and Applications of Multilayered Structures*, edited by P. Dhez and C. Weisbuch (Plenum Press, New York, 1988).
31. I.K. Schuller, *Phys. Rev. Lett.* **44** (1980) p. 1597.
32. G.A. Prinz, *J. Magn. Magn. Mater.* **100** (1991) p. 469.
33. B.T. Jonker, J.J. Krebs, and G.A. Prinz, *Phys. Rev. B* **39** (1989) p. 1399.
34. Y.U. Idzerda, B.T. Jonker, W.T. Elam, and G.A. Prinz, *J. Appl. Phys.* **67** (1989) p. 5385.
35. W.F. Egelhoff Jr., I. Jacob, J.M. Rudd, J.F. Cochran, and B. Heinrich, *J. Vac. Sci. Technol. A* **8** (1990) p. 1582.
36. V. Matijasevic and M.R. Beasley, in *Metallic Superlattices, Artificially Structured Materials*, edited by T. Shinjo and T. Takada (Elsevier, Amsterdam, 1987) p. 187.
37. D.H. Lowndes, D.P. Norton, and J.D. Budai, *Phys. Rev. Lett.* **65** (1990) p. 1160.
38. J-M. Triscone, Ø. Fischer, O. Brunner, L. Antognazza, A.D. Kent, and M.G. Karkut, *Phys. Rev. Lett.* **64** (1990) p. 804.
39. S.J. Pennycook, M.F. Chisholm, D.E. Jenson, D.P. Norton, D.H. Lowndes, R. Feenstra, H.R. Kerchner, and J.O. Thomson, *Phys. Rev. Lett.* **67** (1991) p. 765.
40. E.E. Fullerton, J. Guimpel, O. Nakamura, and I.K. Schuller, *Phys. Rev. Lett.*, in press.
41. For an early report see, for instance, M.A. Beno, L. Soderholm, D.W. Capone II, D.G. Hinks, J.D. Jorgensen, I.K. Schuller, C.U. Segre, K. Zhang, and J.D. Grace, *Appl. Phys. Lett.* **51** (1987) p. 57.
42. For a review see, for instance, I.K. Schuller and J.D. Jorgensen, *MRS Bulletin* **XIV** (2) (1989) p. 27.
43. J.A. Bain, L.J. Chyung, S. Brennan, and B.M. Clemens, *Phys. Rev. B* **44** (1991) p. 1184.
44. A. Fartash, M. Grimsditch, E.E. Fullerton, and I.K. Schuller, *Phys. Rev. B*, in press. □